HETERO-/HOMOGENEOUS REACTION OF HYDROGEN COMBUSTION OVER PLATINUM IN MICRO-CHANNELS

Junjie CHEN*[1], Xuhui GAO[2]

Hetero-/homogeneous combustion of fuel-lean hydrogen-air mixtures in catalytic plane micro-channels was investigated. The main objective is to assess the relative significance of homogeneous reaction as compared with heterogeneous reaction for different dimensions, inlet mass fluxes and equivalence ratios. Results indicated that catalytic walls contribute to sustain homogeneous reaction at micro-scales by decreasing heat losses to wall, and also restrain homogeneous reaction by extracting radicals. Furthermore, the detailed radical chain reaction mechanisms can be significantly changed by the presence of heterogeneous reaction, and radical accumulation in the gas phase can be restrained as a consequence.

Keywords: micro-combustion; homogeneous combustion; heterogeneous combustion; chemical kinetic mechanisms; micro-channels

1. Introduction

Recently, micro-combustion has attracted increased attention due to the growing interests in developing micro-power generation systems [1]. Although pure homogeneous combustion can be stabilized in micro-channels, which are defined as channels with height smaller than 1.0 mm, increasing surface-to-volume ratios render heterogeneous combustion the preferred route compared with pure homogeneous case. Catalytic reaction can broaden the flammability limits and lead to stable combustion even in the presence of high heat losses [2].

There are many challenges to sustain stable combustion at micro-scales: the mass and heat transfers on the wall play a significant role in defining the combustion characteristics with decreasing the characteristic dimension [3]; the increased heat losses can significantly restrain homogeneous reaction [4]. Many useful strategies such as heat-recirculating combustors [5] have been proposed to improve combustion stability and thermal efficiency. Several other efforts have been also employed to sustain homogeneous combustion [6].

Several numerical and experimental investigations [7] have been performed to study the hetero-/homogeneous combustion behavior in catalytic micro-channels. Ghermay et al. [8] investigated the impact of gas-phase chemistry

[1] Associate Prof., School of Mechanical and Power Engineering, Henan Polytechnic University, Jiaozuo, Henan, China, e-mail: comcjj@163.com; comcjj@gmail.com
[2] School of Mechanical and Power Engineering, Henan Polytechnic University, Jiaozuo, Henan, China

in hetero-/homogeneous combustion of hydrogen over platinum. The results delineated the gas-phase conversion of hydrogen could not be ignored. Li et al. [9] investigated the enhancement and combustion characteristics of blended fuels in catalytic micro-channels. They found that the homogeneous combustion can be subsequently ignited and anchored in the cavity, and cavities can further stabilize and enhance homogeneous flame. Khandelwal et al. [10] experimentally investigated the homogeneous combustion behavior in micro-combustors with three rearward facing steps. They proposed that the region of recirculation created due to the sudden expansion at the rearward step aids in stabilizing the homogeneous combustion and can significantly improve the flame stability limits. Fanaee and Esfahani [11] analyzed the effects of main parameters on homogeneous combustion under catalytic and non-catalytic conditions. The results showed that the effect of catalytic surface on expanding homogeneous combustion limits in a lean mixture is larger than the rich one. Bagheri et al. [12] investigated the flame stability of lean premixed hydrogen-air mixture in micro-combustors with different shapes of bluff body. The results showed that the presence of bluff body can expand the flame stability limits.

Key factors such as heat losses, equivalence ratio, thermal conductivity, flow rate, and mixture temperature play a significant role in defining the interaction between homogeneous and heterogeneous reactions, which were discussed in previous studies. As the micro-combustors dimension is decreased, the effects of aforementioned parameters can also be very different. In this work, the relative importance of hetero-/homogeneous reaction associated with lean hydrogen micro-combustion over platinum at different channel heights, inlet mass fluxes, and equivalence ratios are assessed. In order to fully consider effects of the minor species in determining the hetero-/homogeneous reaction pathways, detailed hetero-/homogeneous reaction mechanisms of hydrogen-air are employed.

2. Numerical models and simulation approach

A schematic view of plane micro-channel geometry is shown in Fig. 1. The FLUENT coupled with the CHEMKIN was used to simulate the fluid flow in the plane micro-channel of height H =0.8 mm, length L = 8.0 mm, and solid wall (SiC) thickness δ = 0.1 mm. The plane geometry implies that the third dimension (width) of this micro-channel is assumed infinite, i.e., much larger than the gap size. Inner horizontal surfaces contained platinum catalyst washcoat (properties are shown in Table 1). The incoming hydrogen-air flow was fully premixed with the initial temperature of T_{in} = 300 K and equivalence ratio of φ = 0.4, unless otherwise stated. The fuel-air equivalence ratio of a system is defined as the ratio of the fuel-to-oxidizer ratio to the stoichiometric fuel-to-oxidizer ratio.

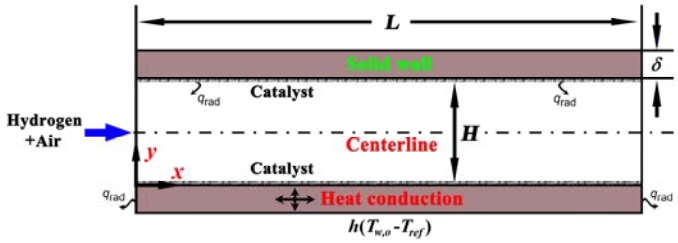

Fig. 1. Schematic diagram of the plane micro-channel geometry

Table 1

The properties of platinum catalyst layer

Property	Value	Reference
catalyst surface site density Γ (mol/cm^2)	2.7×10^{-9}	[13]
average pore diameter d_{pore} (m)	2.6×10^{-8}	[14] and [15]
catalyst porosity ε_{cat}	0.4	[14] and [16]
catalyst tortuosity τ_{cat}	8.0	[14] and [17]
thickness d (μm)	2.0	[14] and [18]

The governing equations for steady, laminar, reactive flow are as follows:Continuity equation:

$$\frac{\partial(\rho u)}{\partial x}+\frac{\partial(\rho v)}{\partial y}=0 \tag{1}$$

Momentum equation:

$$\frac{\partial(\rho uu)}{\partial x}+\frac{\partial(\rho vu)}{\partial y}+\frac{\partial p}{\partial x}-\frac{\partial}{\partial x}\cdot\left[2\mu\frac{\partial u}{\partial x}-\frac{2}{3}\mu\left(\frac{\partial u}{\partial x}+\frac{\partial v}{\partial y}\right)\right]-\frac{\partial}{\partial y}\left[\mu\left(\frac{\partial u}{\partial y}+\frac{\partial v}{\partial x}\right)\right]=0 \tag{2}$$

$$\frac{\partial(\rho uv)}{\partial x}+\frac{\partial(\rho vv)}{\partial y}+\frac{\partial p}{\partial y}-\frac{\partial}{\partial x}\left[\mu\left(\frac{\partial v}{\partial x}+\frac{\partial u}{\partial y}\right)\right]-\frac{\partial}{\partial y}\cdot\left[2\mu\frac{\partial v}{\partial y}-\frac{2}{3}\mu\left(\frac{\partial u}{\partial x}+\frac{\partial v}{\partial y}\right)\right]=0 \tag{3}$$

Energy equation:

$$\frac{\partial(\rho uh)}{\partial x}+\frac{\partial(\rho vh)}{\partial y}+\frac{\partial}{\partial x}\cdot\left(\rho\sum_{k=1}^{k_g}Y_k h_k V_{k,x}-\lambda\frac{\partial T}{\partial x}\right)+\frac{\partial}{\partial y}\cdot\left(\rho\sum_{k=1}^{k_g}Y_k h_k V_{k,y}-\lambda\frac{\partial T}{\partial y}\right)=0 \tag{4}$$

Gas phase species equations:

$$\frac{\partial(\rho uY_k)}{\partial x}+\frac{\partial(\rho vY_k)}{\partial y}+\frac{\partial}{\partial x}\left(\rho Y_k V_{k,x}\right)+\frac{\partial}{\partial y}\left(\rho Y_k V_{k,y}\right)-\dot{w}_k W_k=0,\ k=1,2,\ldots K_g \tag{5}$$

Surface species coverage equations:

$$\frac{\partial\Theta_m}{\partial t}=\sigma_m\frac{\dot{s}_m}{\Gamma},\ m=1,2,\ldots m_s \tag{6}$$

In the above equations x and y are the spatial coordinates parallel and perpendicular to the surface, u and v the corresponding velocity components, λ and μ are the thermal conductivity and viscosity of the mixture respectively, p is the pressure, ρ is the gas density, T is the temperature, h is the total enthalpy of the mixture, Y_k, $\dot{w}_k$, W_k, and h_k are the mass fraction, molar production rate, molecular

weight, and enthalpy of the kth gas phase species respectively, K_g is the total number of gas phase species, and $V_{k,x}$, $V_{k,y}$ are the x- and y-components of the kth species diffusion velocity. Finally, Θ_m, σ_m, and $\dot{s}_m$ denote the coverage, the number of occupied surface sites, and the molar production rate of the mth surface species, respectively; the total number of surface species is M_s. Since heat transfer along the wall significantly affects flame stability, heat transfer in the solid phase is considered. The appropriate energy equation is given as follow:

$$\frac{\partial\left(\lambda_s \partial T\right)}{\partial x^2}+\frac{\partial\left(\lambda_s \partial T\right)}{\partial y^2}=0 \tag{7}$$

where λ_s represents the thermal conductivity of solid wall.

Homogeneous chemical kinetics was described by the detailed mechanism of Konnov et al. [19]. The oxidation of hydrogen over platinum was described by the detailed scheme of Deutschmann et al [20]. The capacity of these schemes to reproduce measured hetero-/homogeneous ignition characteristics has been demonstrated in [21, 22]. Thermodynamic properties and Hetero-/homogeneous reaction rate were evaluated using CHEMKIN and Surface-CHEMKIN, while the transport properties were computed using CHEMKIN's transport library.

The inlet boundary conditions were uniform profiles for the temperature, the axial velocity and the species compositions. Zero gradient Neumann boundary conditions are used at the outlet for all gas phase variables and the no-slip condition at the wall for both velocity components. The radiation between the inner wall surfaces was considered using the discrete ordinates model. At the exterior wall surfaces, heat losses to the surroundings were calculated as follow:

$$q=h\left(T_{w,o}-T_{ref}\right)+\varepsilon\sigma\left(T_{w,o}^4-T_{ref}^4\right) \tag{8}$$

where q is the heat flux, h is the external heat transfer coefficient, $T_{w,o}$ is the outer wall temperature, T_{ref} is the reference temperature, ε is the surface emissivity, and σ is the Stephan-Boltzmann constant (5.67×10^{-8} W/(m^2·K^4)).

3. Results and discussion

3.1. Effect of channel height

Fig. 2 shows H_2 conversion rates at different channel heights, keeping the inlet mass flux J = 0.4 kg/m^2·s constant. Gaseous conversion rates decrease with decreasing the channel height. Initially, as the channel height is reduced from 1.2 to 0.6 mm, the gaseous conversion rates gradually decrease because of the reduced channel volume, while the catalytic conversion rates remain essentially constant. However, there is a precipitous decline in the gaseous conversion rates as the channel height is further reduced. The catalytic conversion rates also slightly increase for the channel height below 0.6 mm because of the reduced gaseous conversion rates. Smaller channels promote catalytic conversion through enhanced transverse mass transfer but also slightly shift the homogeneous flame location (which is defined as the axial position with the highest gaseous

conversion rate) upstream through enhanced transverse heat transfer. The latter inhibits catalytic conversion because the fuel is consumed earlier in the gas phase. Overall, the enhanced transverse mass-transfer rates dominate, and the intensity of catalytic conversion slightly increases with decreasing channel height, but the gaseous conversion decreases.

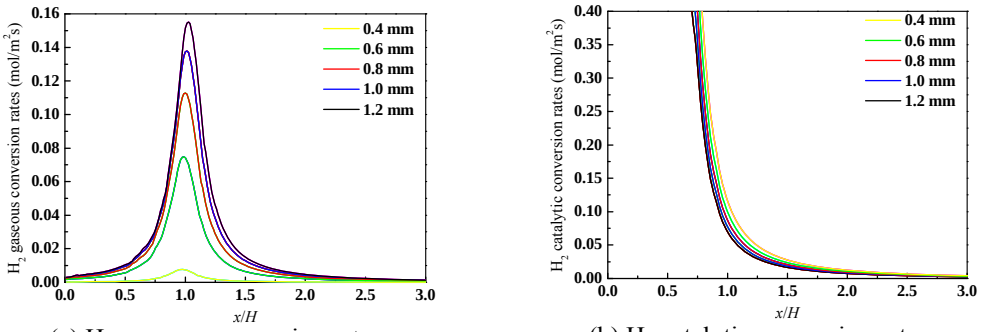

(a) H_2 gaseous conversion rates (b) H_2 catalytic conversion rates

Fig. 2. H_2 conversion rates at different channel heights.

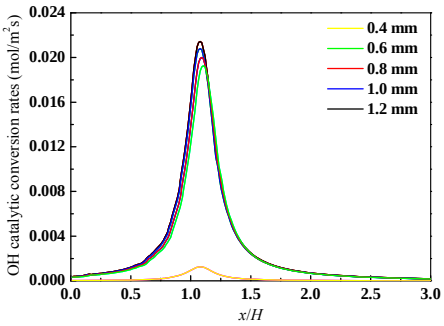

Fig. 3. OH catalytic conversion rates at different channel heights.

OH destruction rate s_{OH} on the wall also exhibits very interesting trend as shown in Fig. 3. As the channel height is reduced from 1.2 mm to 0.6 mm, the OH destruction rate s_{OH} on the wall remains almost constant despite the reduced OH concentrations in the gas phase. Three different reaction modes are employed to assess the effect of wall radical destruction on the homogeneous reactions constraint. They are Case A: Normal simulation, Case B: Lower H_2O effect in homogeneous reactions mechanism (artificial reduction of the H_2O third-body efficiency), and Case C: OH adsorption/desorption reactions are removed from the heterogeneous reactions mechanism.

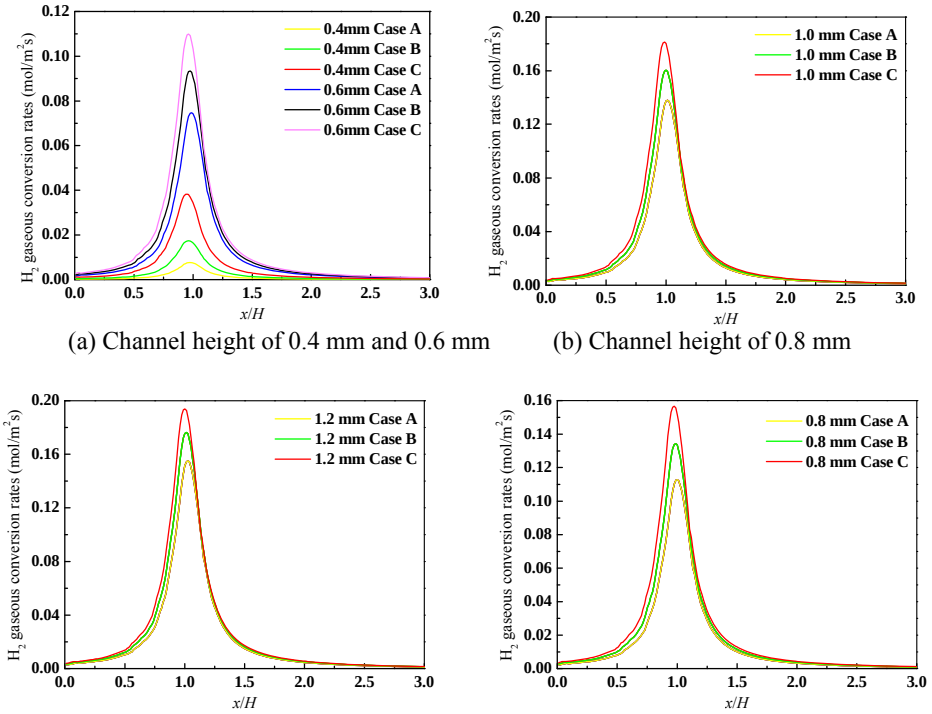

(a) Channel height of 0.4 mm and 0.6 mm (b) Channel height of 0.8 mm

(c) Channel height of 1.0 mm (d) Channel height of 1.2 mm

Fig. 4. H_2 gaseous conversion rates at different channel heights

Fig. 4 shows H_2 gaseous conversion rates for three reaction modes at different channel heights. OH radical destruction on the wall significantly inhibits the gaseous conversion rates. OH adsorption/desorption reactions are mostly important at smaller channels, and the effect gradually diminishes with increasing the channel height. However, in contrast to the effect of the wall OH adsorption/desorption reactions on the maximum gaseous conversion rates, the latter's axial location is only slightly shifted upstream and is not sensitive.

The inlet mass flux is comprised of the convective and diffusion mass flux. As the channels dimension is decreased, the diffusive mass transfer generally becomes more significant [23]. Fig. 5 shows H_2 and H_2O inlet mass fractions at different channel heights. As the channels height is decreased, the H_2 average inlet mass fraction generally decreases as a result of the stronger diffusive mass flux especially in the vicinity of the catalytic wall at lower channel height, while the H_2O average inlet mass fraction increases because of the stronger diffusion effect at lower channel height. However, dissimilar the monotonic trend of hydrogen, the H_2O inlet mass fractions close to the catalytic wall is higher in larger channels.

This behavior occurs because of the relatively smaller diffusion coefficient of H_2O as compared with H_2. The diffusive flux J_{H2O} is responsible for the removal of the reaction products H_2O from the catalytic wall. In larger channels, the diffusive flux J_{H2O} is not strong enough to wash away H_2O from the catalytic wall. Therefore, right at the inlet, a significant difference of H_2O mass fractions exists between the catalytic wall and mid-plane. Decreasing the channel height enhances the diffusive transfer of the reaction products H_2O from the catalytic wall to the gas phase, which in turn decreases the above difference. This increase in the reaction products and decrease in fuel levels at the inlet alters the reaction rates.

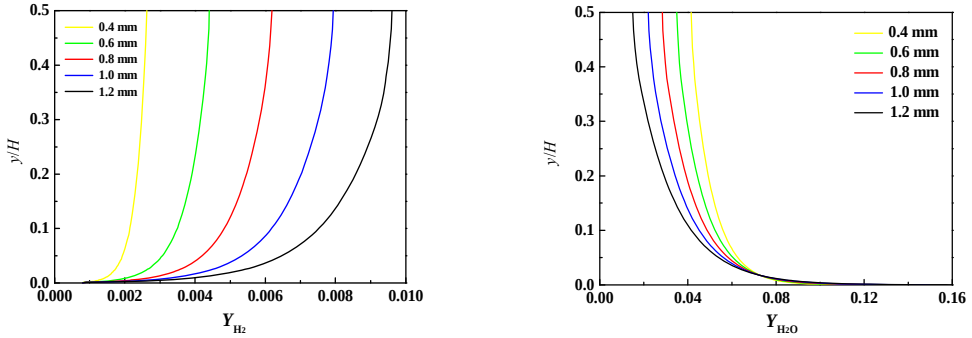

(a) H_2 inlet mass fraction (b) H_2O inlet mass fraction

Fig. 5. H_2 and H_2O inlet mass fractions across the plane channels at different channel heights

Experimental investigations have demonstrated that the presence of H_2O inhibits homogeneous reactions [24-26]. As a chain terminating reaction, $H + O_2 + H_2O = HO_2 + H_2O$ is a significant elementary reaction step. In order to assess the effect of the H_2O-induced suppression on the gaseous conversion rates, the above reaction is removed from the surface reactions mechanism. The gaseous conversion rates with (Case A) and without (Case B) the above reaction are shown in Fig. 4. The presence of H_2O inhabits the homogeneous reactions. For example, in the 0.6 mm channel, the peak value of the gaseous conversion rates is about 24.8% greater in the simulation of the artificially reduced H_2O third-body efficiency (Case B) compared to the results of the normal simulation (Case A). However, in the smallest channel, effect of the H_2O-induced inhibition on the homogeneous reactions is much smaller than the catalytic wall OH destruction.

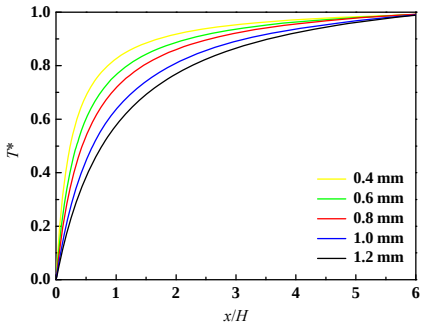

Fig. 6. Non-dimensional mid-plane temperature at different channel heights

The non-dimensional mid-plane temperature T^* [$T^* = (T - T_{in})/(T_w - T_{in})$] profiles at different channel heights are shown in Fig. 6. Mid-plane temperature increases with decreasing the channel height because of stronger diffusion effect at smaller channel height. Elevated temperatures promote the gaseous conversion rates because of the reaction rates are strong functions of temperature. However, the temperature variation as a result of the channel dimension change does not seem to have a significant effect on the gaseous conversion rates as previously observed. In other words, the rise in gas temperature as a result of the channel dimension is not strong enough to compete with the other suppressing effects.

3.2. Effect of mass flux

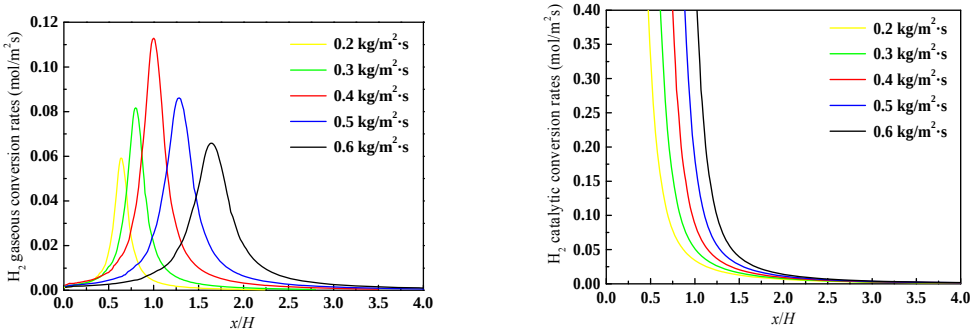

(a) H_2 gaseous conversion rates (b) H_2 catalytic conversion rates

Fig. 7. H_2 conversion rates along the plane channel at different inlet mass flow fluxes

The change in the inlet mass flux alters the relative significant of the diffusive and convective mass fluxes which can affect the reactive flow behavior. The streamwise profile of H_2 conversion rates at different inlet mass flow fluxes are shown in Fig. 7. Gaseous conversion rates initially increases as the inlet mass flow flux is increased and then decreases as the mass flow flux is further increased. However, catalytic conversion rates increase as the inlet mass flow flux is increased. Upon increasing the inlet mass flux, the homogeneous chemistry ignition might move first upstream because of the increased power input that

enhances combustion. Subsequently, it is pushed downstream as a result of the fast advection of the cold inlet gases, which prolongs the time for the heat released at the wall to raise the bulk gas to the ignition temperature, and the increased heat losses from the extended preheating/combustion zone, which should be compensated by additional fuel consumption at the catalytic wall. All things considered, the former effect dominates at smaller inlet mass fluxes in Figure 7a, where gaseous conversion is promoted; the latter dominates at larger inlet mass fluxes in Figure 7a, where gaseous conversion is slightly inhibited.

The H(s) and H_2O(s) surface coverage at different inlet mass fluxes are shown in Fig. 8. With increasing mass fluxes, there is increased finite rate chemistry, which in turn leads to higher levels of $\Theta_{H(s)}$ and $\Theta_{H_2O(s)}$. The relative gaseous and catalytic contribution are shown in Table 2. The catalytic conversion dominance is apparent in all cases. As the inlet mass flux is increased, H_2 supply to the channel increases linearly, while the relative gaseous contribution rapidly decreases to the negligible levels. The amount of gaseous conversion initially increases as the inlet mass flux is increased and then decreases as the inlet mass flux is further increased. Due to the highly non-linear interactions between the convection and diffusion fluxes, transport properties and chemical kinetics, one should not expect the linear behavior in catalytic conversion rates.

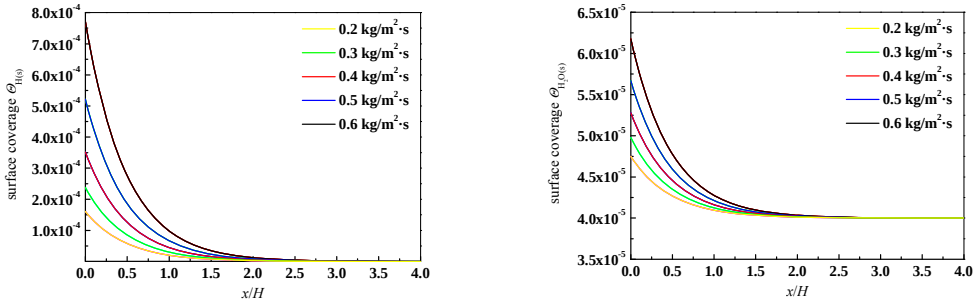

(a) H(s) surface coverage (b) H_2O(s) surface coverage

Fig. 8. H(s) and H_2O(s) surface coverage along the plane channel at different inlet mass fluxes

Table 2

H_2 conversion rates along the plane channel at different inlet mass fluxes

J (kg/m^2·s)	0.2	0.3	0.4	0.5	0.6
Gaseous contribution (×10^6 kg/s)	0.047	0.084	0.098	0.088	0.062
Catalytic contribution (×10^6 kg/s)	0.744	1.208	1.722	2.448	3.346
Percentage of gaseous contribution (%)	9.8	8.2	6.4	4.4	2.2
Percentage of catalytic contribution (%)	90.2	91.8	93.6	95.6	97.8

The cross-stream H_2 mass fraction profiles at axial locations of maximum gaseous conversion are shown in Fig. 9. The trend observed in the available H_2 for homogeneous reaction is consistent with the gaseous contribution observed in Table 2 and Fig. 7. Initially, as the inlet mass flux is increased, the available H_2

for homogeneous reaction also increases. However, as the inlet mass flux further increases, the increased catalytic conversion depletes the available H_2 in the gas phase, which inhibits the gaseous conversion. The variety in the inlet mass flux also affects the temperature field, which can restrain the gaseous conversion rates in turn. As the inlet mass flux increases, the temperature at every axial location decreases as shown in Fig. 10 where the non-dimensional mid-plane temperature profiles are shown. Therefore, as the inlet mass flux increases, besides the decline in the available H_2 for homogeneous combustion, the lower temperature levels also restrain the homogeneous combustion.

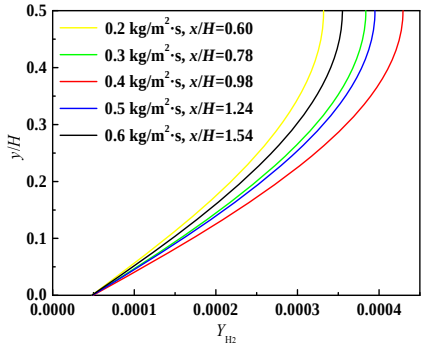

Fig. 9. Cross-stream H_2 mass fraction profiles at axial locations of maximum gaseous conversion

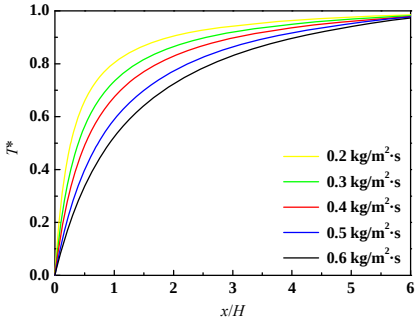

Fig. 10. Non-dimensional mid-plane temperature at different inlet mass fluxes

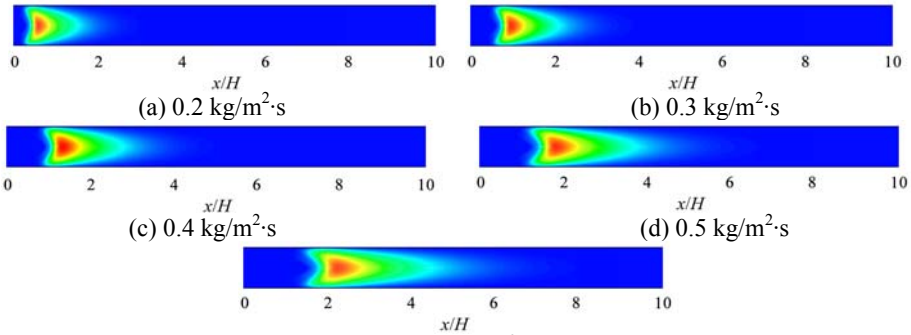

(a) 0.2 kg/m^2·s (b) 0.3 kg/m^2·s

(c) 0.4 kg/m^2·s (d) 0.5 kg/m^2·s

(e) 0.6 kg/m^2 s

Fig. 11. OH mass fractions along the 0.8 mm plane channel at different inlet mass fluxes

OH mass fraction contours at different inlet mass fluxes are shown in Fig. 11. Initially, as the inlet mass flux is increased from 0.2 to 0.4 kg/m^2·s, the OH mass fraction also increases. However, as the inlet mass flux further increases, the OH mass fraction level drops sharply. This behavior is consistent with the homogeneous reaction levels of H_2 at different inlet mass fluxes as observed earlier in Fig. 7 (a), Fig. 9, and Table 2. The higher gas phase contribution to H_2 conversion can produce more OH radical in the gas phase. As the inlet mass flux is increased, the location of the highest OH mass fraction slightly shifts downstream, and the region of homogeneous reaction stretched along the channel.

3.3. Effect of equivalence ratio

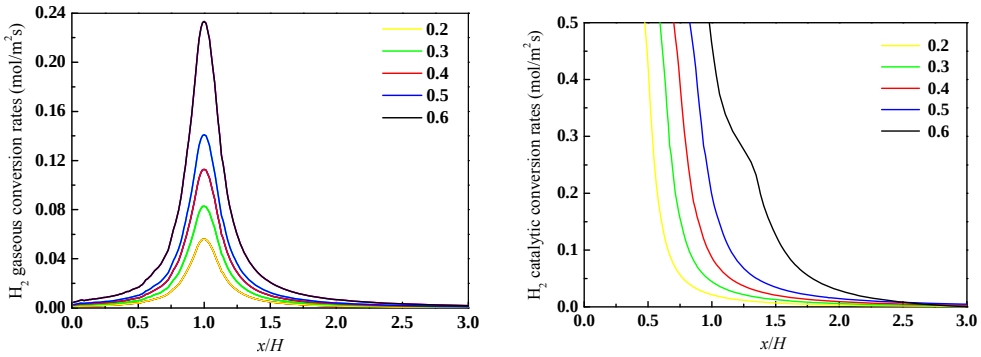

(a) H_2 gaseous conversion rates (b) H_2 catalytic conversion rates

Fig. 12. H_2 gaseous and catalytic conversion rates along the 0.8 mm channel at different inlet equivalence ratios

For the low equivalence ratios case, the reaction rates are generally lower because of the absence of enough fuel. This result can be confirmed in Fig. 12 where the gaseous and catalytic conversion rates are depicted. For relatively fuel-richer mixtures case, both gaseous and catalytic conversion rates are higher as expected. The increase in the relative homogeneous contribution can be apparently detected at φ = 0.6 by observing the sudden decline in the catalytic conversion rates. As the H_2 gets depleted mainly through the heterogeneous reaction, fuel-leaner mixtures exhibit the monotonic decrease in the catalytic conversion rates. However, for the higher inlet equivalence ratio case, as the homogeneous reaction initiates, the sudden decline occurs in the catalytic conversion rates due to the gaseous consumption becomes significant.

In order to examine the relative homogeneous contribution at different equivalence ratios, the H_2 mass fraction distribution across the channel with and

without considering homogeneous reaction is shown in Fig. 13. In relatively fuel-richer mixtures, the error associated with neglecting the homogeneous reaction is much higher. This effect can also be confirmed by observing the entire conversion behavior. The H_2 consumption in relatively fuel-richer mixtures are shown in Fig. 14. Close to the inlet section, the two simulations predict almost identical results due to H_2 is mostly consumed by the heterogeneous reaction. However, as the homogeneous reaction initiates, the difference in H_2 consumption predictions becomes apparent.

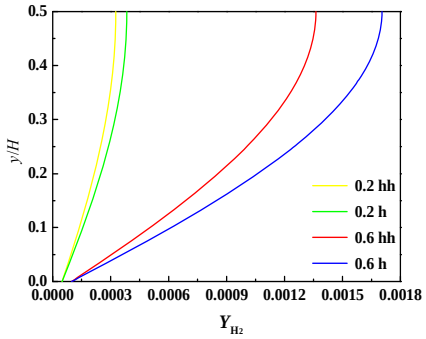

Fig. 13. H_2 mass fraction profiles across the 0.8 mm channel at $x/H = 0.98$ and different inlet equivalence ratios, wherein hh: hetero-/homogeneous reaction, h: heterogeneous reaction alone

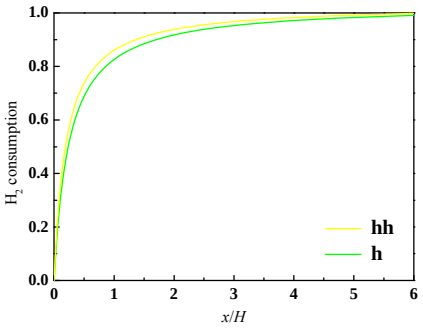

Fig. 14. H_2 consumption with inlet equivalence ratio $\varphi = 0.6$ along the 0.8 mm plane channel

4. Conclusions

Homogeneous contribution reduces with decreasing the channel height. As the channel height is decreased from 1.2 to 0.6 mm, the decline in gaseous conversion rates is gradual, and is primarily due to the decreased channel volume and the increased OH radical adsorption. The OH radical destruction continues to restrain the homogeneous reaction even further in smaller channels. In this range, the catalytic conversion rates remain essentially constant. As the channel dimension is decreased, the upstream diffusion of the product species from the channel towards the inlet section becomes significant as a result of the stronger

diffusive mass flux in smaller channels. The above effect leads to the existence of the product species, which contributes even further to decline in the gaseous conversion rates at the inlet section as the channel below the 0.6 mm.

Variation of inlet mass flux alters the balance between diffusive and convective mass fluxes. The presence of product species suppresses the gaseous conversion rates at low inlet mass fluxes. As the inlet mass flux increases, initially the amount of gaseous conversion also increases. However, after the certain inlet mass flux, this trend reverses and the increased inlet mass flux results in lower gaseous conversion rates. As the inlet mass flux increases, catalytic conversion rates increase steadily mainly due to the steeper gradients on the catalytic wall, and the relative homogeneous contribution rapidly declines to the negligible levels.

Finally, the equivalence ratio significantly effects the homogeneous reaction contribution. At low equivalence ratio, the gaseous and catalytic conversion rates are generally lower as a result of the absence of enough fuel, compared with the relatively fuel-richer case. As the equivalence ratio is increased but below the stoichiometric mixture, both gaseous and catalytic conversion rates increase, although the increase of gaseous conversion rates is more vigorous.

Acknowledgments

This work was supported by the National Natural Science Foundation of China (No. 51506048).

REFERENCES

[1] *D. Fernandez-Galisteo, C. Jimenez, M. Sanchez-Sanz, and V.N. Kurdyumov*. The differential diffusion effect of the intermediate species on the stability of premixed flames propagating in microchannels. *Combustion Theory and Modelling*, **Vol. 18**, no. 4-5, 2014, pp.582-605.

[2] *A. Brambilla, C.E. Frouzakis, J. Mantzaras, A. Tomboulides, S. Kerkemeier, and K. Boulouchos*. Detailed transient numerical simulation of H_2/air hetero-/homogeneous combustion in platinum-coated channels with conjugate heat transfer. *Combustion and Flame*, **Vol. 161**, no. 10, 2014, pp. 2692-2707.

[3] *E. Miyata, N. Fukushima, Y. Naka, M. Shimura, M. Tanahashi, and T. Miyauchi*. Direct numerical simulation of micro combustion in a narrow circular channel with a detailed kinetic mechanism. *Proceedings of the Combustion Institute*, **Vol. 35**, no. 3, 2015, pp.3421-3427.

[4] *M. Nakahara, F. Abe, K. Tokunaga, and A. Ishihara*. Effect of dilution gas on burning velocity of hydrogen-premixed meso-scale spherical laminar flames. *Proceedings of the Combustion Institute*, **Vol. 35**, no. 1, 2015, pp.639-646.

[5] *G.P. Gauthier, G.M.G. Watson, and J.M. Bergthorson*. Burning rates and temperatures of flames in excess-enthalpy burners: A numerical study of flame propagation in small heat-recirculating tubes. *Combustion and Flame*, **Vol. 161**, no. 9, 2014, pp.2348-2360.

[6] *F. Bianco, S. Chibbaro, and G. Legros*. Low-dimensional modeling of flame dynamics in heated microchannels. *Chemical Engineering Science*, **Vol. 122**, 2015, pp.533-544.

[7] *B. Yenerdag, N. Fukushima, M. Shimura, M. Tanahashi, and T. Miyauchi*. Turbulence-flame interaction and fractal characteristics of H_2-air premixed flame under pressure rising condition. *Proceedings of the Combustion Institute*, **Vol. 35**, no. 2, 2015, pp.1277-1285.

[8] *Y. Ghermay, J. Mantzaras, R. Bombach, and K. Boulouchos*. Homogeneous combustion of fuel-lean $H_2/O_2/N_2$ mixtures over platinum at elevated pressures and preheats. *Combustion and Flame*,

Vol. 158, no. 8, 2011, pp. 1491-1506.
[9] *Y.H. Li, G.B. Chen, F.H. Wu, T.S. Cheng, and Y.C. Chao*. Effects of catalyst segmentation with cavities on combustion enhancement of blended fuels in a micro channel. *Combustion and Flame*, **Vol. 159**, no. 4, 2012, pp. 1644-1651.
[10] *B. Khandelwal, A.A. Deshpande, and S. Kumar*. Experimental studies on flame stabilization in a three step rearward facing configuration based micro channel combustor. *Applied Thermal Engineering*, **Vol. 58**, no. 1-2, 2013, pp. 363-368.
[11] *S.A. Fanaee and J.A. Esfahani*. Two-dimensional analytical model of flame characteristic in catalytic micro-combustors for a hydrogen-air mixture. *International Journal of Hydrogen Energy*, **Vol. 39**, no. 9, 2014, pp. 4600-4610.
[12] *G. Bagheri, S.E. Hosseini, and M.A. Wahid*. Effects of bluff body shape on the flame stability in premixed micro-combustion of hydrogen air mixture. *Applied Thermal Engineering*, **Vol. 67**, no. 1-2, 2014, pp. 266-272.
[13] *O. Deutschmann, R. Schmidt, F. Behrendt, and J. Warnatz*. Numerical modeling of catalytic ignition. *Symposium (International) on Combustion*, **Vol. 26**, no. 1, 1996, pp. 1747-1754.
[14] *I. Sen and A.K. Avci*. Simulation of exhaust gas reforming of propane in a heat exchange integrated microchannel reactor. *International Journal of Hydrogen Energy*, **Vol. 39**, no. 2, 2014, pp. 844-852.
[15] *X. Karatzas, J. Dawody, A. Grant, E.E. Svensson, and L.J. Pettersson*. Zone-coated Rh-based monolithic catalyst for authothermal reforming of diesel. *Applied Catalysis B: Environmental*, **Vol. 101**, no. 3-4, 2011, pp. 226-238.
[16] *A.K. Avci, D.L. Trimm, and M. Karakaya*. Microreactor catalytic combustion for chemicals processing. *Catalysis Today*, **Vol. 155**, no. 1-2, 2010, pp. 66-74.
[17] *R.E. Hayes, S.T. Kolaczkowskib, P.K.C. Li, and S. Awdry*. Evaluating the effective diffusivity of methane in the washcoat of a honeycomb monolith. *Applied Catalysis B: Environmental*, **Vol. 25**, no. 2-3, 2000, pp. 93-104.
[18] *M. Karakaya and A.K. Avci*. Microchannel reactor modeling for combustion driven reforming of *iso*-octane. *International Journal of Hydrogen Energy*, **Vol. 36**, no. 11, 2011, pp. 6569-6577.
[19] *A.A. Konnov*. Remaining uncertainties in the kinetic mechanism of hydrogen combustion. *Combustion and Flame*, **Vol. 152**, no. 4, 2008, pp. 507-528.
[20] *O. Deutschmann, L.I. Maier, U. Riedel, A.H. Stroemman, and R.W. Dibble*. Hydrogen assisted catalytic combustion of methane on platinum. *Catalysis Today*, **Vol. 59**, no. 1-2, 2000, pp. 141-150.
[21] *A. Brambilla, C.E. Frouzakis, J. Mantzaras, R. Bombach, and K. Boulouchos*. Flame dynamics in lean premixed CO/H_2/air combustion in a mesoscale channel. *Combustion and Flame*, **Vol. 161**, no. 5, 2014, pp.1268-1281.
[22] *X. Zheng and J. Mantzaras*. An analytical and numerical investigation of hetero-/homogeneous combustion with deficient reactants having larger than unity Lewis numbers. *Combustion and Flame*, **Vol. 161**, no. 7, 2014, pp. 1911-1922.
[23] *C.-H. Leu, S.-C. King, J.-M. Huang, C.-C. Chen, S.-S. Tzeng, C.-I. Lee, W.-C. Chang, and C.-C. Yang*. Visible images of the catalytic combustion of methanol in a micro-channel reactor. *Chemical Engineering Journal*, **Vol. 226**, 2013, pp.201-208.
[24] *C. Appel, J. Mantzaras, R. Schaeren, R. Bombach, A. Inauen, B. Kaeppeli, B. Hemmerling, and A. Stampanoni*. An experimental and numerical investigation of homogeneous ignition in catalytically stabilized combustion of hydrogen/air mixtures over platinum. *Combustion and Flame*, **Vol. 128**, no. 4, 2002, pp. 240-368.
[25] *Y. Ghermay, J. Mantzaras, and R. Bombach*. Effects of hydrogen preconversion on the homogeneous ignition of fuel-lean $H_2/O_2/N_2/CO_2$ mixtures over platinum at moderate pressures. *Combustion and Flame*, **Vol. 157**, no. 10, 2010, pp. 1942-1958.
[26] *D.G. Norton, and D.G. Vlachos*. Hydrogen assisted self-ignition of propane/air mixtures in catalytic microburners. *Proceedings of the Combustion Institute*, **Vol. 30**, no. 2, 2005, pp. 2473-2480.